# Broadband coupling scattering of all-dielectric conical multimer nanostructures

BO FANG[a], WEIMIN WANG[b,c], XUFENG JING[b,c,*], QIAN ZOU[d], CHENXIA LI[b,#], XIYONG ZOU[b], ZHI HONG[c]
[a]*College of Metrology & Measurement Engineering, China Jiliang University, Hangzhou 310018, China*
[b]*Institute of Optoelectronic Technology, China Jiliang University, Hangzhou 310018, China*
[c]*Centre for THz Research, China Jiliang University, Hangzhou 310018, China.*
[d]*Jinan Vocational College, Jinan, China*

We numerically simulated the broadband scattering with electric and magnetic dipoles resonance on coupled dimeric and trimeric silicon nanocones. A single silicon nanocone shows the relatively narrow band electric and magnetic resonance scattering. The dimeric silicon nanocones indicate a mixed resonant mode, and the resonant scattering bandwidth is increased. These scattering optical responses are clarified by their scattering cross section and the spatial distributions of electromagnetic fields. Moreover, the scattering bandwidth of silicon nanotrimer is further increased.Interestingly, a new magnetic resonant mode emerges at longer wavelength. Broadband resonant scattering results from optically magnetic coupling interaction between trimeric silicon nanocones.The effect of different particle diameter, shape and substrate on the scattering resonance of the electric dipole and magnetic dipole modes is numerically investigated for single, dimeric and trimeric silicon nanocones.

(Received September 13, 2018; accepted April 8, 2019)

*Keywords:* Nanoparticles, Electromagnetic scattering, Dielectric, Nanostructures

## 1. Introduction

On the account of the development of nanotechnology, the ability to manipulate light at nanoscale is of great importance for future optical chip integration. The resonant nanostructures have a large scattering cross section and are therefore suitable to concentrate, redirect and manipulate light. Generally,the plasma nanoparticles werefrequently used for sensing, imaging [1, 2], focusing and scattering light in solar cell [3, 4] and light emitting devices [5, 6]. Compared with metallic nanoparticles dominated by the electric resonance, the high refractive index dielectric nanoparticles exhibit electric resonance and magnetic resonance [7,8]. Unlike plasma particles, electromagnetic resonances of dielectric nanoparticles are driven by displacement current rather than actual current [9]. Thus, these resonant nanoparticles are characterized by low loss [10-13], especially, in visible and infrared regions.

So far, most studies have focused on single high-refractive-index dielectric nanoparticle [14,15] or unit cell structure that is still a periodic array of individual nanoparticle [16,17]. Recently, the interaction [18-22] between high refractive index dielectric nanoparticles was explored [10,19] to the angular radiation pattern by the electric and the magnetic resonance. It is known that most investigations of resonant behavior of nanoparticles concentrated on nanospheres, nanobricks, and nanodisks, and so on [18,19,25]. There is no systematic study of the effect of particle geometry and dielectric environment on the resonant properties of dielectric nanocones. These subwavelength nanocones with unique characteristics, such as broadband antireflection and directional scattering[8], will exhibit distinct resonant performance compared with other shape. Moreover, for practical applications in optical devices, nanoparticles should be placed on substrate, and in most cases it is even desirable to strongly couple to the substrate (e.g., absorption in photodiodes [24], solar cells [25,26], etc.). This interaction with substrate strongly affects the resonant behavior of particles. Therefore, the investigation of the coupled effect of nanocones with substrate is necessary and important for practical application.

In this work, we use the finite-difference time-domain (FDTD [27,28]) method to numerically study the resonant scattering properties of silicon nanocones. The resonant electromagnetic dipole scattering for single, dimeric, and trimericnanocones is systematically analyzed. The mutual effect between nanocones and the interaction with substrate are detailedly revealed. When decreasing the gap size between nanocones, the interactionstrength changes from weak to strong. In the case of dimeric or trimeric nanocomposites, the strong magnetic-magnetic interaction produces a new magnetic resonance mode, showing a wideband scattering characteristic compared to a single nanocone. In addition, the presence of (high

refractive index) substrates significantly influences the resonant properties and the interaction between different intrinsic modes. This broadband response in dielectric nanocones can be effectively applied innanophotonics devices [29-32] or metamaterias devices [33-42], such as nano-antennas and solar cells.

## 2. Simulation results and discussions

### 2.1. Scattering properties of single silicon nanocone

We use finite-difference time-domain simulation (FDTD) to calculate the normalized scattering cross section (normalized to the cross-section of the geometric cross section) and the field distribution inside the particle. The FDTD method belongs in the general class of grid-based differential numerical modeling methods (finite difference methods). The time-dependent Maxwell's equations (in partial differential form) are discretized using central-difference approximations to the space and time partial derivatives. A total field scattered field source is used, and a wide-band (λ=600-1400 nm) plane wave is launched from the top at normal incidence. The power of the scattered field can be monitored by the power transmission monitors which are positioned around the total field scattered field source. The electromagnetic field distribution is monitored by field monitors placed in and around the nanoparticles. We use perfectly matching layers to prevent any scattering from the simulation boundaries. Automatic non-uniform meshes are used, and a 2.5 nm refinement mesh around the particle is used when monitoring the near-field intensities. The recognition of the resonance is performed by studying the field distribution inside the particles.

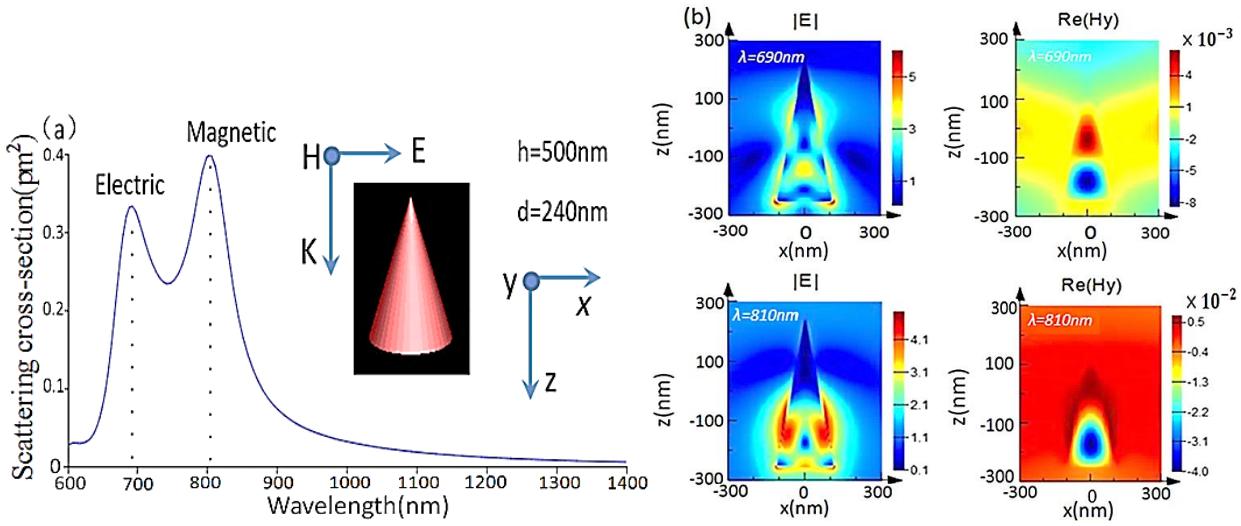


*Fig. 1. (a) Scattering cross section of single silicon nanocone. Electromagnetic resonancesare indicated by dashed lines. The corresponding nanoconesstructure is shown in the inset with the height of 500nm and the diameter of 240nm. (b) The electric field intensity ($|E|$) distribution in the x-z plane and the magnetic field ($H_y$) distribution, the magnetic resonance at λ=801nm and the electrical resonance at λ=690nm, respectively.The units for the electric and magnetic fields are V/m and A/m, respectively*

We firstly study the scattering spectrum of single silicon nanocone as shown in Fig. 1 (a) with the height of 500nm and the diameter of 240nm. The obvious electric dipole resonance near λ=690nm and magnetic dipole resonance at about λ=801nm are indicated by the dotted lines, respectively. In order to clearly understand the magnetic and electric dipole resonance modes, the electric field intensity ($|E|$) distribution and the magnetic field ($H_y$) distribution in x-z planewere numerically simulated in Fig. 1 (b). From the electric field distribution (left column), we observe a linear electric field distribution at λ=690nm and a displacement current loop associated with a circulating electric field at λ=801nm. In the right column for the magnetic field distribution in Fig. 1 (b), there is a node at the center at λ=690nm, which is consistent with an electric dipole. At λ=801nm, an antinode at the center is observed, which is consistent with a magnetic dipole. All these observations indicate that the resonant mode at λ=690nm results from electrical resonance, and the resonant mode at λ=801nm is derived from the magnetic resonance.

In short, the in-plane magnetic dipole is driven by an electric field coupled to the displacement current loop in the vertical direction of the particle. The displacement current loop causes a magnetic dipole moment perpendicular to the direction of polarization of the

electric field. The effective driving of such a displacement current loop requires a significant delay in the driving field of the entire particle since the electric field should undergo a significant phase shift to match the opposing electric field orientation in the top and bottom of the particle [13]. So it is expected that the magnetic dipole resonance cannot be excited with smaller height of nanocones. On the other hand, the excitation of the electric dipole resonance only requires that material within the resonator ispolarized collectively by electric field components of the incident light.

### 2.2. Scattering of dimeric silicon nanocones

In the following section, we study the influence of the interaction between two nanocones on the scattering properties. Fig. 2 shows the scattering spectra of dimeric silicon nanoconeswith gap size from 20nm to 200 nm. In the case of large gap of g = 200 nm, the scattering spectrum similar to that of the single silicon nanocones corresponding to a weak interaction is obtained. It is worth noting that the absolute value of its scattering amplitude is significantly larger than the scattering value of a single silicon nanocone. The larger scattering peak for dimeric silicon nanocones with the gap of g = 200 nm may be attributed to the superposition of scattering amplitude for two nanoparticles at the resonant wavelength. As the gap decreases, we observe that the electric and magnetic resonances become closer to each other, and the electric resonance becomes less pronounced.

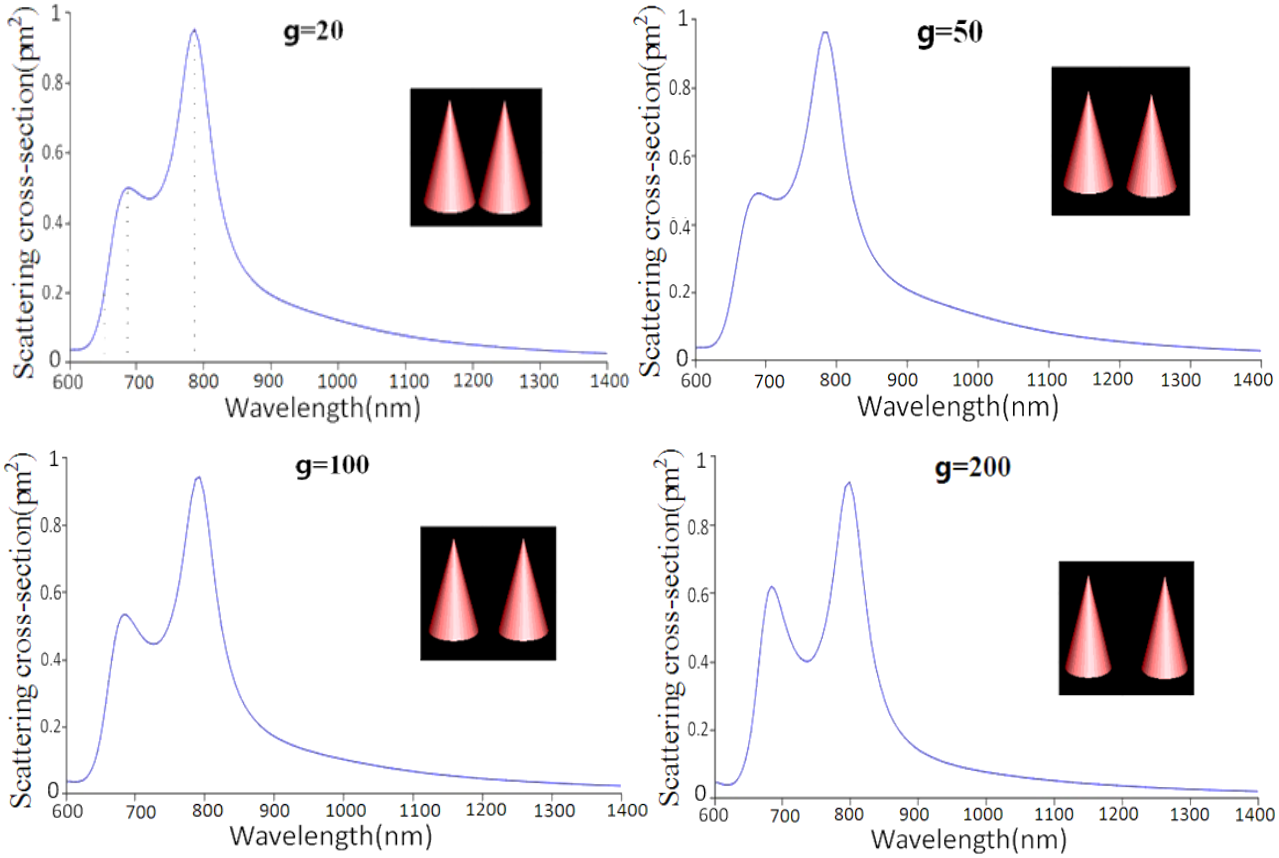


*Fig. 2. The scattering spectra of dimers with the gap varying from 20 nm to 200 nm. Two silicon nanocones are the same ( $d$ = 240nm and $h$ = 500nm)*

In order to clearly understand the interaction of electric resonance and magnetic resonance in dimericnanocones, the intensity distributions of electric field and magnetic field are numerically simulated respectively with the gap of 20nm as shown in Fig. 3. From the scattering spectrum, we select three spectral positions of three dashed lines: the mode deviating from the magnetic and electric resonance at λ=650 nm, the electric resonance mode at λ = 690 nm, and the magnetic resonance mode at λ = 775 nm. In the cross-sectional view at λ = 650 nm, the electric field and the magnetic field show respectivelyan antinode and a node in the center, showing the electric dipole properties consistent with those in Fig. 1 (b). Due to the interaction of nanocones, the field distribution at λ = 690 nm exhibits a slightly distorted electric resonance. At λ = 775 nm, we observe that the electric field exhibits a displacement current loop, and the magnetic field shows a node, leading to magnetic dipole resonance. It should be noted that the field distribution in the dimericnanocones

exhibits an asymmetric feature relative to that of single nanocone. Thus, the electric and magnetic resonances move closer to each other to form a hybrid resonant mode.

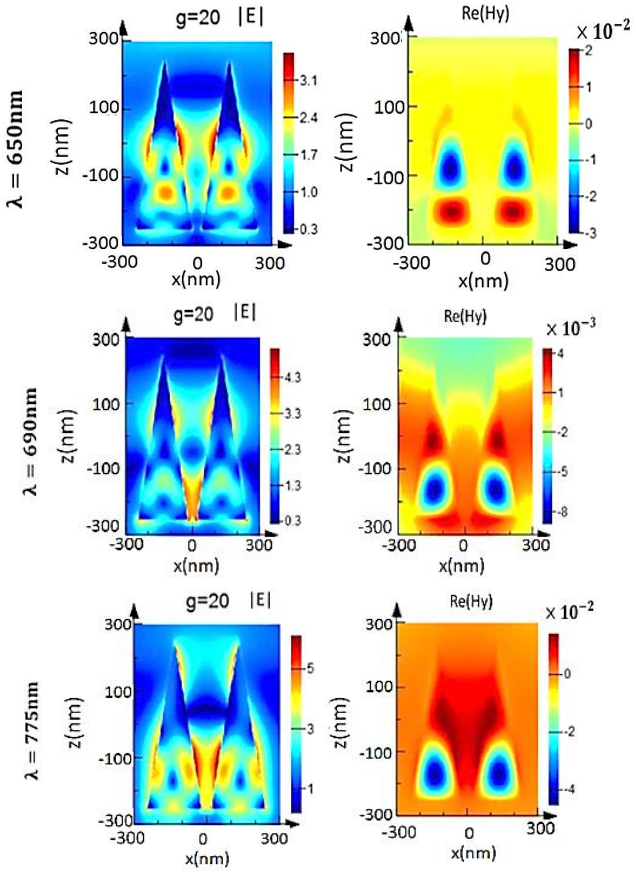


*Fig. 3. The intensity distribution of the electric field (| E |) and the magnetic field (| $H_y$ |) of the dimer with the gap g= 20 nm atλ= 650 nm, λ= 690 nm and λ= 775 nm at x-z plane. The units for the electric and magnetic fields are V/m and A/m, respectively*

By analyzing the magnitude of the field strength, the interaction of two nanocones is more complex and more powerful than the single nanocone structure, which can be obtained by comparing the field distribution of both. And we can clearly see that the electric field intensity near the bottom of nanocone is significantly larger than the apex, while the electric field and magnetic field strength at λ = 650nm and λ = 690nm is close to zero at the apex. Due to the amplitude of magnetic and electric field are higher at λ= 775 nm, so the scattering cross section is higher than that for λ = 650nm and λ = 690nm.

### 2.3. Broadband scattering of trimeric silicon nanocones

Next, it will be shown that the trimeric silicon nanocones can introduce an even more complex interaction. Fig. 4 shows the scattering spectra of trimeric silicon nanocones with the gap of g= 20nm and g= 60nm, respectively. In the case of g= 20nm, it corresponds to a strong interaction, and an obvious magnetic resonance splitting occurs. However, we can find a slight downward trend near $\lambda$ =800nm, which is due to strong interactions that may be detrimental in practical applications. In order to avoid the occurrence of this phenomenon, we can increase the gap between trimmers. At g= 60nm,the trimershows relatively continuous broadband response, and the newly emerging magnetic resonance mode is almost invisible in the case of weak coupling.

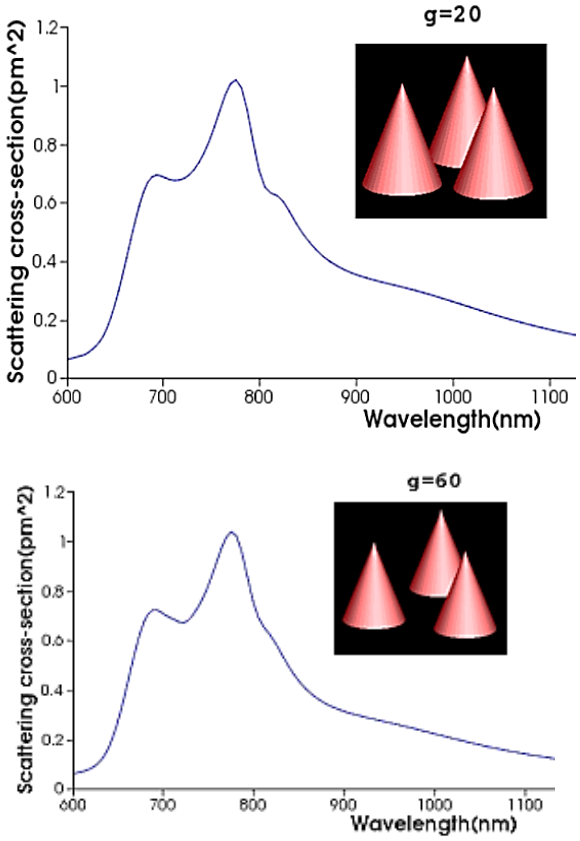


*Fig. 4. Scattering spectrum of trimer ( $d$ = 240 nm and $h$ = 500 nm) with gap g= 20 nm (left) and g= 60 nm (right)*

### 2.4. Influence of nanoparticle height and substrate

Fig. 5 shows the scattering cross-section of singlenanocone as a function of the height with the diameter of d = 240 nm. In Fig. 5 (a), the silicon nanocone is in air. The blue shift of the electric and magnetic resonances can be observed with decrease of height, and the amplitude of both electric dipole resonance and magnetic dipole resonance is decreased. These resonant properties are clearly different from that of nanodisks [13]. When the nanocone is on the substrate of $SiO_2$, the resonant performance is similar to that in air as a function of height. In Fig. 5 (b), it can be seen that

the scattering spectrum of the electric and magnetic resonances are widen compared with the nanocone in air, which is attributed to the extension of the partial pattern to the substrate. The displacement current loop may extend into substrate when the dielectric resonator is on the substrate.

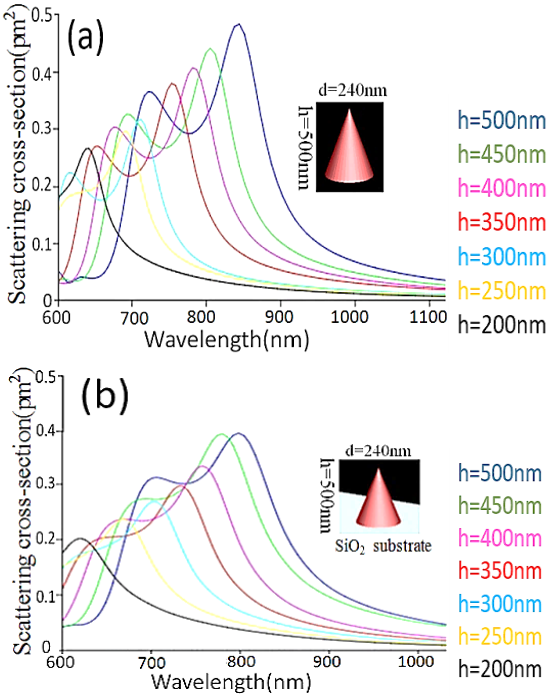


*Fig. 5. (a) The scattering cross section as a function of the nanostructure height with the diameter d = 240 nm in air, (b) on the substrate of $SiO_2$*

### 2.5. Substrate refractive index and particle shape effect

It has been previously shown that when the conical resonator is on a silica substrate, the electric resonance and the magnetic resonance are broadened. Next, we examine the resonant response at different substrate. Fig. 6 shows that the scattering cross section ofsingle silicon cone with d = 240 nm and h = 500 nm located on a semi-infinite substrate with refractive index of $1 \leq n_{sub} \leq 4$.

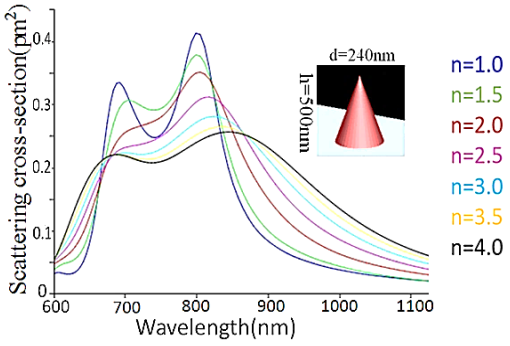


*Fig. 6. The scattering cross section ofsinglesilicon cone with h = 500 nm and d = 240 nm on semi-infinite substrate for $1 \leq n_{sub} \leq 4$*

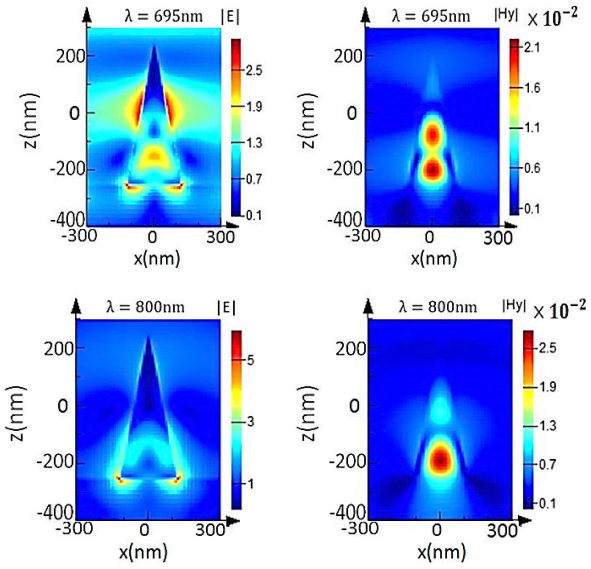


*Fig. 7. The electromagnetic fields of electromagnetic resonance at λ=695nm and λ=800nm, respectively. The refractive index of the substrate is n = 1. The units for the electric and magnetic fields are V/m and A/m, respectively*

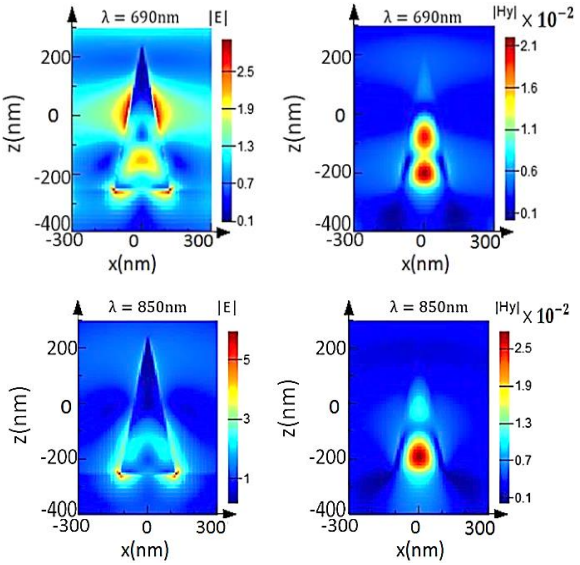


*Fig. 8. The electromagnetic fields of electromagnetic resonance at λ=690nm and λ=850nm, respectively. The refractive index of the substrate is n = 4. The units for the electric and magnetic fields are V/m and A/m, respectively*

As observed in Fig. 6, the substrate refractive index is gradually increased from 1 to 4, leading to the enhancement of bandwidth for electric resonance and the magnetic resonance. The electric resonance mode gradually becomes the shoulder of the magnetic resonance mode. It can be seen that when is increased, the magnetic resonance peak is significantly reduced due to an increase in the local density of the optical state at the particle location. The resonance position of magnetic dipole is more sensitive on substrate refractive index than that of electric dipole. By the way, in the plasma

resonance, most of the light is at the interface (in direct contact with the substrate). As observed in Fig. 7 and Fig. 8, we can get a better coupling with the substrate when the substrate refractive index is closer to the resonator (at n = 4),and the decrease in the magnitude of the magnetic resonance peak. But, in the case of a metal resonator, most of the light is concentrated inside the resonator, making it less sensitive to the refractive index of the substrate.

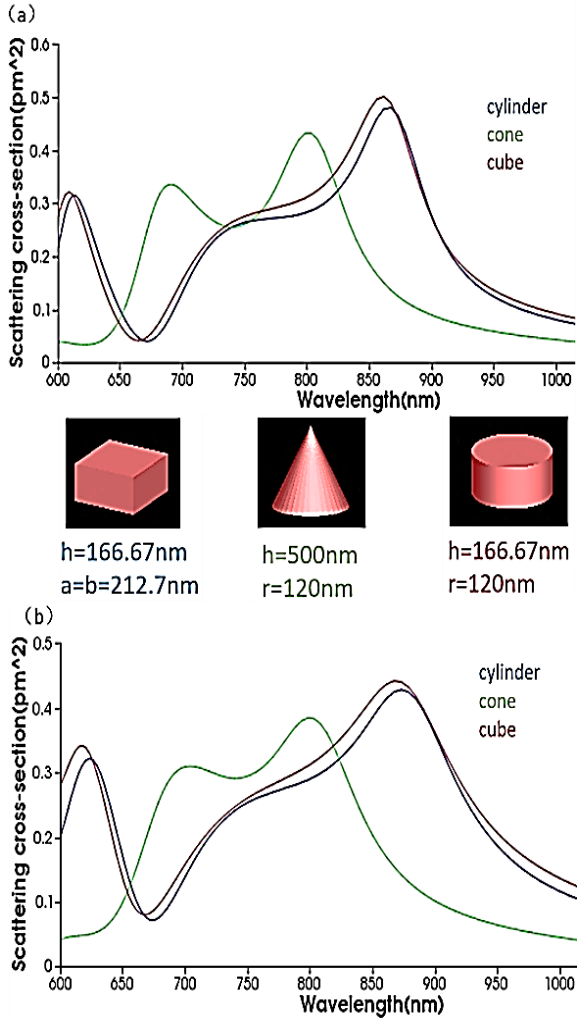


*Fig. 9. (a) The scattering cross section of the cylinder, cone and rectangular parallelepiped in air; (b) On semi-infinite silica substrate. All nanoparticles are composed of Si, and they have the same volume and maintain the same bottom area*

In order to study the effect of particle shape on the resonant response, Fig. 9 shows the scattering cross section of the cone (green curve), the cylinder (blue curve) and the rectangular parallelepiped (red curve) as a function of wavelength. The particles have the same volume and have the same bottom area.All nanoparticles are made of Si material, and the geometry is shown in the middle of Fig. 9. Regardless of the structure, the amplitude of resonant peaks in air is lower than that on substrate. The resonant characteristics for nanocones are obviously different from that of nano-cylinder and nano-parallelepiped. This unique resonant performance of nanoconescan be distinctively applied in nanophotonics elements.

### 2.6. Periodic array of silicon nanocones

It can be seen from Fig. 10 (a) that the reflection peaks of periodic arrays of individual silicon nanocomposites appear at $\lambda$ = 675 nm and $\lambda$ = 755 nm, respectively, indicating significant resonances at these two wavelengths. However, with silicon dioxide substrate, the electric and magnetic resonances occur at $\lambda$ =720 nm and $\lambda$ = 800 nm, respectively. The overall reflectivity of more than 80% at the wavelength range from 720nm to 800nm can be obtained for nanocones array with substrate. This configuration can be applied to broadband reflection device with all dielectric nanostructure. In Fig. 11, the reflection peaks of the periodic arrays of dimeric silicon nanocomposites appear at $\lambda$ = 725 nm and $\lambda$ =820 nm, respectively, indicating a significant resonance.Unlike the resonant properties exhibited by the single-cone periodic structure, the interaction in the dimeric nanocone periodic structure results in obvious electromagnetically induced transparency at 770nm.

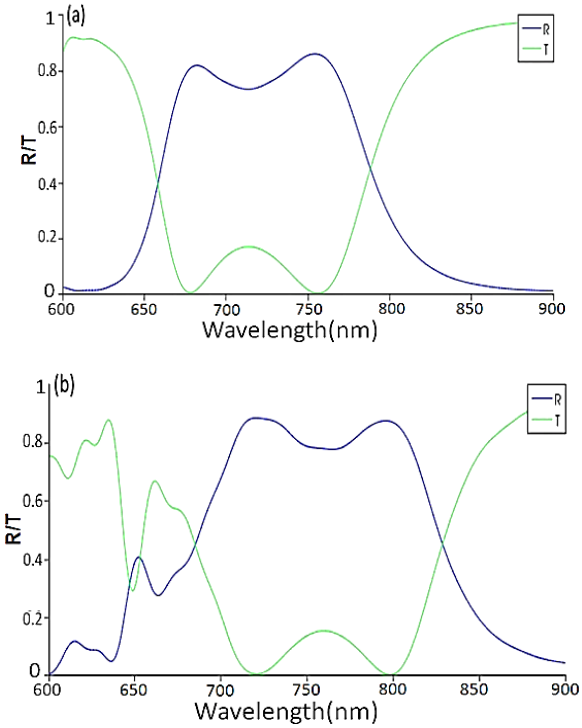


*Fig. 10. The transmission and reflection of the periodic array of individual silicon nanocone in (a) the air and (b)under a semi-infinite substrate respectively, where the substrate material is silicon dioxide.The silicon cone is d = 240 nm, h = 500 nm*

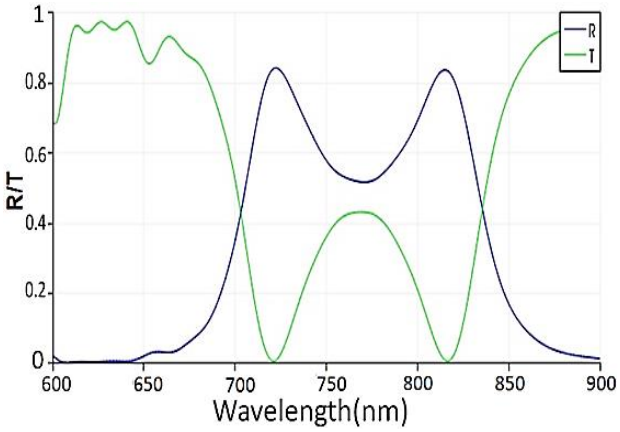


*Fig. 11. The transmission and reflection of periodic array of double silicon nanocones in air, the silicon cone is d = 240 nm, h = 500 nm, the spacing between the two cones is g = 300 nm. R denotes reflectance curve, and T denotes transmittance curve*

## 3. Conclusion

In summary, we systematically study scattering resonant properties of nanocones. The broadband scattering properties of dimeric and trimeric silicon nanocones are numerically calculated. As the gap between the dimers decreases, we can see that the magnetic resonance and electricresonance are close to each other, resulting in a mixed pattern. The trimeric silicon nanocones introduce stronger interaction, resulting in further increase in bandwidth. The dimer and trimer with substrate exhibit a significant increase in continuous bandwidth compared to single silicon nanocomposite. The periodic arrays of nanocones indicate a significant resonance response.

### Acknowledgements

The authors acknowledge the support from National Key R&D Program of China (No. 2018YFF01013005), Natural Science Foundation of Zhejiang Province (LY17F050009), National Natural Science Foundation of China (NSFC) (No.61875159).

## References

[1] J. A. Schuller, E. S. Barnard, W. Cai, Y. C. Jun, J. S. White, M. L. Brongersma, Nat. Mater. **9**(3), 193 (2010).
[2] C. Hoppener, L. Novotny, Nano Lett. **8**(2), 642 (2008).
[3] H. A. Atwater, A. Polman, Nat. Mater. **9**(3), 205 (2010).
[4] V. E. Ferry, M. A. Verschuuren, H. B. T. Li, E. Verhagen, R. H. Walters, R. E. I. Schropp, H. A. Atwater, A. Polman, Opt. Express **18** Suppl. **2**(13), A237 (2010).
[5] M. K. Kwon, J. Y. Kim, B. H. Kim, I. K. Park, C. Y. Cho, C. C. Byeon, S. J. Park, Adv. Mater. **20**(7), 1253 (2010).
[6] N. Yu, R. Blanchard, J. Fan, Q. J. Wang, C. Pflugl, L. Diehl, T. Edamura, M. Yamanishi, H. Kan, F. Capasso, Opt. Express **16**(24), 19447 (2008).
[7] H. Xue, T. Giang, T. Sunil, C. Nic, Photon. Res. **6**(10), 981 (2018).
[8] W. Chen, J. Zhang, B. Peng, Ö. Kaya, X. Fan, L. Yang, Photon. Res. **6**(5), A23 (2018).
[9] Y. H. Fu, A. I. Kuznetsov, A. E. Miroschnichenko, Y. F. Yu, B. Lukyanchuk, Nat. Commun. **4**(2), 1527 (2013).
[10] A. B. Evlyukhin, C. Reinhardt, A. Seidel, B. S. Lukyanchuck, B. N. Chichkov, Phys. Rev. B **82**(4), 2181 (2010).
[11] A. B. Evlyukhin, S. M. Novikov, U. Zywietz, R. L. Eriksen, C. Reinhardt, S. I. Bozhevolnyi, B. N. Chichkov, Nano Lett. **12**(7), 3749 (2012).
[12] J. A. Schuller, M. L. Brongersma, Opt. Express **17**(26), 24084 (2009).
[13] A. I. Kuznetsov, A. E. Miroschnichenko, Y. H. Fu, J. B. Zhang, B. Lukyanchuk, Sci. Rep. **2**(7), 492 (2012)
[14] N. T. Fofang, T. S. Luk, M. Okandan, G. N. Nielson, I. Brener, Opt. Express **21**(4), 4774 (2013).
[15] J. van de Groep, A. Polman, Opt. Express **21**(22), 26285 (2013).
[16] J. C. Ginn, I. Brener, D. W. Peters, J. R. Wendt, J. O. Stevens, P. F. Hines, L. I. Basilio, L. K. Warne, J. F. Ihlefeld, P. G. Clem, M. B. Sinclair, Phys. Rev. Lett. **108**(9), 097402 (2012).
[17] I. Staude, A. E. Miroshnichenko, M. Decker, N. T. Fofang, S. Liu, E. Gonzales, J. Dominguez, T. S. Luk, D. N. Neshev, I. Brener, Y. Kivshar, ACS Nano **7**(9), 7824 (2013).
[18] F. J. Bezares, J. P. Long, O. J. Glembocki, J. Guo, R. W. Rendell, R. Kasica, L. Shirey, J. C. Owrutsky, J. D. Caldwell, Opt. Express **21**(23), 27587 (2013).
[19] D. S. Filonov, A. P. Slobozhanyuk, A. E. Krasnok, P. A. Belov, E. A. Nenasheva, B. Hopkins, A. E. Miroshnichenko, Y. S. Kivshar, Appl. Phys. Rev. Lett. **104**(2), 2257 (2014).
[20] B. Rolly, B. Bebey, S. Bidault, B. Stout, N. Bonod, Phys. Rev. B **85**, 245432 (2012).
[21] J. Li, X. Zhang, Photon. Res. **6**(6), 630 (2018).
[22] H. T. Tung, D. H. Phuc, Chin. Opt. Lett. **16**(7), 072501 (2018).
[23] I. Staude, A. E. Miroshnichenko, M. Decker, N. T. Fofang, S. Liu, E. Gonzales, J. Dominguez, T. S. Luk, D. N. Neshev, I. Brener, Y. Kivshar, ACS Nano **7**(9), 7824 (2013).
[24] P. Fan, K. C. Y. Huang, L. Cao, M. L. Brongersma, Nano Lett. **13**(2), 392 (2013).

[25] P. Spinelli, M. A. Verschuuren, A. Polman, Nat. Commun. **3**(2), 692 (2012).
[26] P. Spinelli, B. Macco, M. A. Verschuuren, W. M. M. Kessels, A. Polman, Appl. Phys. Lett. **102**(23), 1925 (2013).
[27] A. Taflove, S. C. Hagness, Computational Electrodynamics: The Finite- Difference Time-Domain Method, Lmn. pub. ro, 2005.
[28] C. Wang, Z. Y. Jia, K. Zhang, Y. Zhou, R. H. Fan, X. Xiong, R. W. Peng, J. Appl. Phys. **115**(24), 131 (2014).
[29] A. Ghobadi, Amir, T. Ghobadi, A. K. Okyay, K. Ali, E. Ozbay, Photon. Res. **6**(4), 244 (2018).
[30] L. Gong, B. Gu, G. Rui, Y. Cui, Z. Zhu, Q. Zhan, Photon. Res. **6**(2), 138 (2018).
[31] Y. Cai, J. Wang, J. Zhang, H. Wan, Z. Zhang, L. Zhang, Chin. Opt. Lett. **16**(1), 010602 (2018).
[32] Y. D. Peng, Z. J. Zhang, X. Q. Wang, S. D. Liu, A. H. Yang, X. S. Wang, Opt. Quant. Electron. **50**(8), 311 (2018).
[33] X. Jing, X. Gui, P. Zhou, Z. Hong, J. Lightwave Technol. **36**(12), 2322 (2018).
[34] R. Xia, X. Jing, X. Gui, Y. Tian, Opt. Mater. Express **7**(3), 977 (2017).
[35] X. Gui, X. Jing, Z. Hong, IEEE Photonic Tech. L. **30**(10), 923 (2018).
[36] X. Jing, Q. Ye, Z. Hong, D. Zhu, and G. Shi, Superlattice. Microst. **111**, 830 (2017).
[37] X. Bie, X. Jing, Z. Hong, C. Li, Appl. Opt. **57**(30), 9070 (2018).
[38] X. Gui, X. Jing, P. Zhou, J. Liu, Z. Hong, Appl. Phys. B **124**(4), 68 (2018).
[39] X. Gui, X. Jing, J. Liu, P. Zhou, Z. Hong, Infrared Phys. Tech. **89**, 174 (2018).
[40] J. Zhao, X. Jing, W. Wang, Y. Tian, D. Zhu, G. Shi, Opt. Laser Technol. **95**, 56 (2017).
[41] X. Jing, X. Gui, P. Zhou, Z. Hong, IEEE Photonics J. **9**(1), 5900107 (2017).
[42] J. Mian, H. Zhu, D. Zhu, et al., Optoelectron. Adv. Mat. **11**(3-4), 148 (2017).

*Corresponding author: jingxufeng_1984@163.com
lichenxiacjlu@163.com